



TECHNICAL ARTICLE

Influence of Different Ultraviolet Radiation Intensities on the Corrosion Behavior of Type 316 Stainless Steel in a Simulated Salt-Lake Atmospheric Environment

Mingxiao Guo, Hui Feng, Naeem ul Haq Tariq, Xiaohan Li, Junrong Tang, Chen Pan, and Zhenyao Wang

Submitted: 9 June 2021 / Revised: 12 November 2021 / Accepted: 28 November 2021 / Published online: 27 January 2022

In this study, the influence of different ultraviolet (UV) radiation intensities on the corrosion behavior of 316 stainless steel (316 SS) was investigated using an accelerated test method for simulated salt-lake atmospheric corrosion. The corroded specimens were analyzed using scanning electron microscopy (SEM), laser scanning confocal microscopy (LSCM), x-ray photoelectron spectroscopy (XPS), white light interferometry (WLI), and in situ electrochemical impedance spectroscopy (EIS). The UV radiation restrained the corrosion rate of 316 SS, wherein the influence of UV inhibition initially increased and then decreased when the intensity of UV radiation was increased from 0.25 to 2 mw/cm². The strongest inhibition effect was observed for the UV radiation intensity of 0.5 mw/cm². The inhibition effect on the corrosion rate of 316 SS exposed to UV radiation was related to the protection ability of corrosion products. The protection ability of corrosion products improved with an increase in the ratio of $[Cr]/\{[Cr] + [Fe]\}$. The maximum pit depth and pit density formed on 316 SS initially exhibited a gradual decrease and then an increase in the UV radiation intensity in the range 0.25–2 mw/cm².

Keywords 316 SS, accelerated corrosion, atmospheric corrosion, uv radiation intensity

1. Introduction

Atmospheric corrosion of metals is an electrochemical process that occurs on an aqueous film formed over a metallic surface. The corrosion rate of metals in different atmospheres is influenced by various environmental factors such as temperature (Ref 1–3), relative humidity (RH) (Ref 4, 5), frequency of wet/dry cycles (Ref 6, 7), and air pollutants (Ref 7–10). Metals in the atmosphere are directly exposed to sunlight, which consists of approximately 2% ultraviolet radiation. Consequently, UV radiation is also an indispensable factor that affects the corrosion of different metals in the atmosphere. In recent years, several studies have investigated the influence of UV radiation on the corrosion behavior of metals exposed to the atmosphere. Song *et al.* reported the strong influence of UV radiation on the atmospheric corrosion process (induced by NaCl) of Q235 carbon steel, resulting in a significant increase

in its corrosion rate (Ref 11). Thompson *et al.* found that UV radiation triggered the corrosion activity of Zn-based alloys after exposure for 4 months to the effluents (Ref 12). They observed that the photoinduced electrons migrated to the interface of the electrolyte and accelerated the cathodic reaction, thus accelerating the pitting corrosion of zinc alloys (Ref 12). Liu *et al.* studied the influence of UV radiation intensity on the corrosion behavior of Q235 in the south sea atmosphere and found that a considerable number of holds and fissures were distributed in the corrosion product layer. When the UV radiation intensity is increased to a certain degree, the corrosion rate of carbon steel is accelerated (Ref 13).

In general, stainless steels are widely used in various atmospheric environments owing to their excellent corrosion resistance. Nevertheless, atmospheric corrosion still occurs in these materials, particularly in an aggressive chloride ion environment. Most contemporary research on the effect of UV radiation on the corrosion performance of stainless steel focuses on the bulk electrolyte. Breslin *et al.* investigated the influence of UV radiation on the corrosion behavior of 316 SS in a NaCl solution. They found that the passive film of 316 SS was modified by UV radiation, and the pitting corrosion of 316 SS was improved (Ref 14). Moussa *et al.* proposed that UV radiation can improve the corrosion resistance of 304 SS in chloride-containing solutions and inhibit the pit growth of 304 SS (Ref 15). Stainless steels exposed to the atmosphere receive more UV radiation than those exposed to a solution. Thus, the corrosion behavior of stainless steel in an atmospheric environment is relatively different from that in a solution. However, there are few studies on the corrosion behavior of stainless steel in an atmospheric environment. Therefore, it is of great significance to study the corrosion behavior of stainless steel in the atmosphere.

Mingxiao Guo, Xiaohan Li, and Junrong Tang, Institute of Metal Research, Chinese Academy of Sciences, Shenyang 110016, China; and School of Materials Science and Engineering, University of Science and Technology of China, Shenyang 110016, China; Hui Feng, Chen Pan, and Zhenyao Wang, Institute of Metal Research, Chinese Academy of Sciences, Shenyang 110016, China; and Naeem ul Haq Tariq, Department of Metallurgy and Materials Engineering, Pakistan Institute of Engineering and Applied Sciences, Nilore, Islamabad, Pakistan. Contact e-mails: cpan@imr.ac.cn and zhywang@imr.ac.cn.

The atmosphere of salt lakes, located in the northwest of China, is characterized by arid-rainless conditions and land salinization. Table 1 lists the climatic parameters of a typical salt-lake atmosphere. The high rate of sea salt deposition in this region exacerbates the atmospheric corrosion of metals in the region. Moreover, the salt-lake atmosphere is typically rich in MgCl₂ salt particles with very low RH (*i.e.*, <50%, or even approximately 30% RH), while the marine atmosphere is typically high in RH (> 80% RH). Our previous research has demonstrated that the corrosion rate of stainless steel in a salt-lake environment is higher than that in a marine environment. This is mainly due to the differences in the DRH and ERH values between MgCl₂ and NaCl (Ref 16). However, the influence of UV radiation on the environment was ignored in these studies. Furthermore, the metal in a salt-lake environment is more exposed to UV radiation than that in a marine environment. Thus, it is crucial to examine the influence of UV radiation on the corrosion behavior of 316 SS in a salt-lake environment.

Atmospheric corrosion is an electrochemical process; therefore, real-time atmospheric corrosion monitoring technologies such as atmospheric corrosion monitors (ACM) (Ref 17-19) and Kelvin probes (Ref 20) have been widely employed. However, the practical application of these methods is limited by many factors, some of which are not suitable for actual field monitoring, while others can only provide the severity of the degree of corrosion but not the direct information about existing electrochemical processes. However, *in situ* EIS has been used to obtain direct and real-time data on the corrosion behavior of metals using special micro-distance electrodes. Through this technique, corrosion rates along with the corrosion mechanisms of interface-related phenomena can be estimated (Ref 21-24).

Therefore, based on our previous work (Ref 16), we analyzed the effect of different UV radiation intensities on the corrosion behavior of 316 SS in detail, using *in situ* EIS, SEM, LSCM, WLI, and XPS technologies. For this purpose, the UV radiation intensities were set to 0.25, 0.5, 1, and 2 mW/cm². Furthermore, the effect of UV radiation on the corrosion mechanism of 316 SS is discussed.

2. Experimental

2.1 Samples Preparation and Electrodes Preparation

For the accelerated wet/dry cyclic corrosion test and EIS analysis, specimens with dimensions 50 × 25 × 3 mm³ and 10 × 10 × 3 mm³ were cut from the as-received 316 SS plate. The composition of the 316 SS plates is listed in Table 2. To obtain the electrochemical signals, a comb-like micro-distance electrode was constructed on a 316 SS plate using the same method

outlined in our previous work (Ref 21). The 316 SS specimens were separated by a thin insulating layer and sealed using epoxy resin. Figure 1(a) shows the arrangement of the *in situ* electrodes. Figure 1(b) illustrates the distance (approximately 60 μm) between the two specimens. The micro-distance electrodes were mechanically ground with SiC paper up to 2000 grit and then stored in a dryer for at least 24 h, followed by a wet/dry cyclic corrosion test.

2.2 Wet/Dry Cyclic Corrosion Experiment

To simulate the atmospheric environment of a salt lake, a wet/dry cyclic corrosion experiment was performed using a Weiss-Voetsch temperature and climatic test system (Fig. 2), and the effect of various UV radiation intensities on the corrosion behavior of 316 SS was investigated. The samples in the test chamber were divided into two layers separated by an anti-UV apron. The specimens in the top layer were irradiated with UV radiation, whereas those in the lower layer were not exposed to UV radiation. UV intensity was measured using a UVAB light meter (Tenmars-TM213). The test system was connected to an electrochemical station.

The wet/dry cyclic corrosion experiment was carried out for 10 days to simulate real day and night conditions in the salt-lake environment. The wet/dry cycle included the following steps: (1) wetting the 316 SS surface with 20 μL/cm² of 0.1 mol/L MgCl₂ to simulate a salt-lake environment; (2) drying the surface in an oven maintained at 40 °C; (3) wetting the surface in the test chamber at 30 °C and RH (80%) for 60 min in the absence of UV light; (4) drying the surface in the test chamber fixed at 30 °C and RH (20%) for 120 min under UV light; and (5) repeating steps (3) to (4) 15 times.

2.3 Electrochemical Measurements

The *in situ* EIS test was carried out using a PARSTAT 2273 workstation. The EIS spectra of the micro-distance electrodes, under a thin liquid MgCl₂ film, were measured *in situ* in the corrosion test chamber, as shown in Fig. 2. The amplitude of the AC voltage was maintained at 10 mV. The scanning frequency, which was set between 10⁵ Hz and 10⁻² Hz in the test process, was applied from high to low values during the test, and a total of 50 frequency points were obtained. The *in situ* EIS data were processed using the commercial software “ZSimpWin” (version 3.21).

2.4 Characterization

The two-dimensional (2D) surface morphologies of 316 SS were observed using SEM (XL30-FEG). Three-dimensional (3D) surface morphologies of 316 SS were observed using a non-contact laser scanning confocal microscope (LSCM, Zeiss LSM-700). The surface roughness of the specimens was recorded using LSCM. The composition of the corrosion

Table 1 Climatic parameters of the salt-lake environment.

Mean temperature, °C/year	Mean rainfall, mm/year	Mean evaporation, mm/year	Salt fragments, mg m ⁻² /d	Natural deposition, g m ⁻² /month	
				Soluble	Insoluble
17.5	38.3	3067	19.16	23.19	20.98

Table 2 Chemical compositions of the 316 SS stainless steel (wt.%)

C	P	S	Si	N	Mn	Mo	Cr	Ni	Fe
0.04	0.26	0.002	0.3	0.04	1.28	2.2	16.8	10.7	Bal.

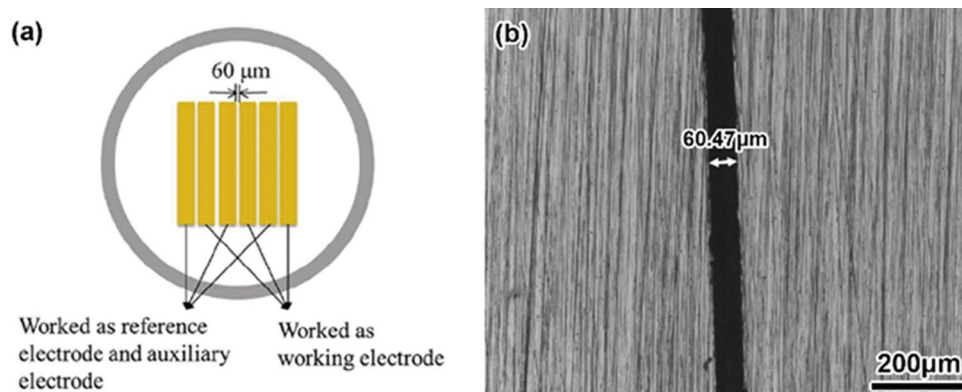


Fig. 1 Schematic diagram electrode design: (a) top view of the comb-like microelectrodes; (b) optical micrograph showing the distance between two plates

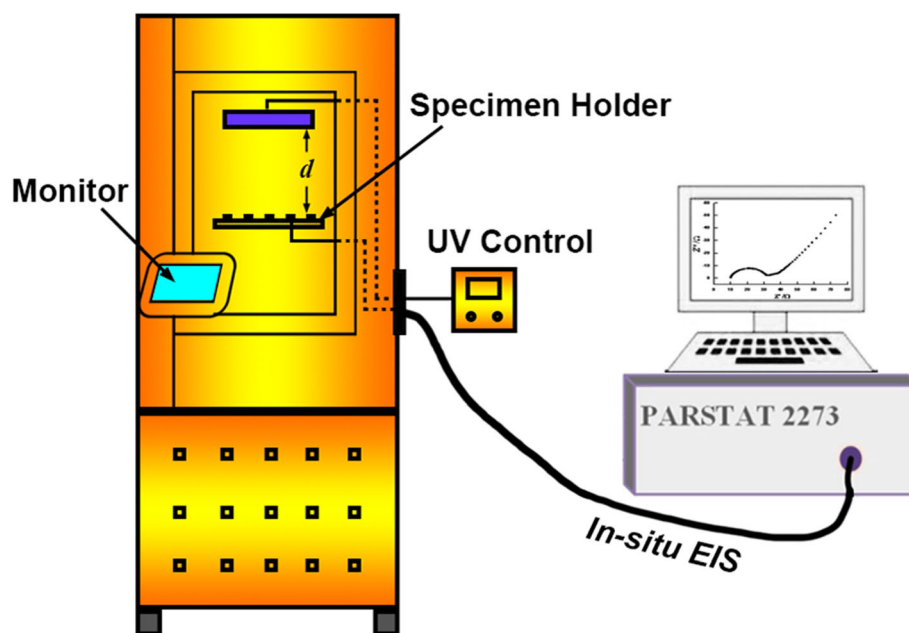


Fig. 2 Schematic diagram elaborating in situ EIS test for performing wet-dry cyclic corrosion experiment under different UV radiation intensities

products was assessed via XPS (ESCALAB 250) using monochromatic Al $K\alpha$ radiation ($h\nu = 1486.6$ eV). For XPS, the measured current of the sample was $2 \mu\text{A}$, and the size of the bombardment zone was $2 \times 2 \text{ mm}^2$. The binding energy (BE) was corrected using a carbon pollution standard (284.6 eV). Finally, XPS data were processed using “XPSPEAK 4.1.”

The corrosion products of 316 SS were carefully removed in a specific chemical solution (100 mL nitric acid + 900 mL distilled water) and vigorously stirred at 60°C for approximately 20 min as per the International Organization for Standardization (ISO) 8407 standard. After removing the corrosion products formed on the surface of 316 SS, the pit morphologies and pit depth statistics were estimated using a

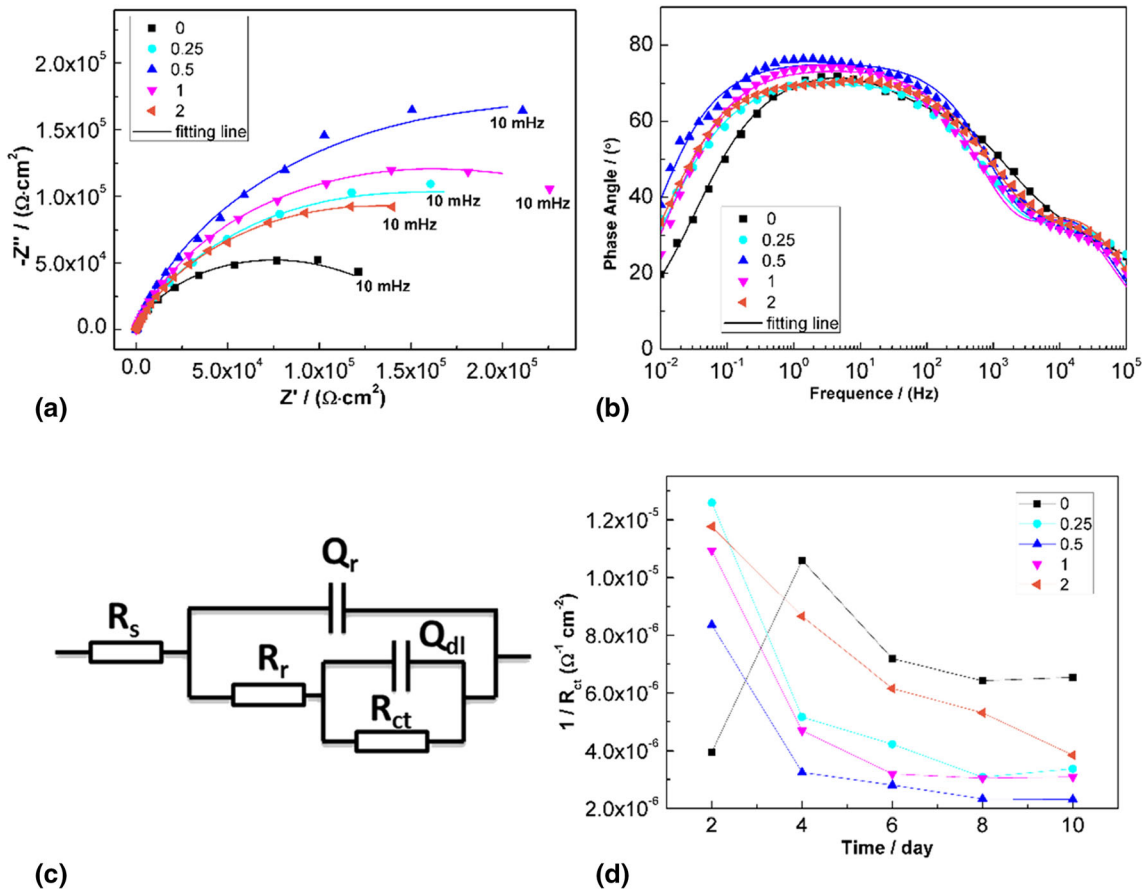


Fig. 3 In situ EIS results of 316 SS under various UV radiation intensities after 10 days of corrosion: (a) Nyquist plot, (b) Bode plot, (c) equivalent circuits, and (d) reciprocal of R_{ct}

white light interferometer (WLI, Micro XAM). The pit density was determined using image analysis software (Image J).

3. Results and Discussion

3.1 In Situ EIS

Figure 3(a) and (b) displays the Nyquist and Bode plots of 316 SS under different UV radiation intensities after 10 days of corrosion. Figure 3(c) shows the equivalent circuit obtained after fitting the in situ EIS results. As shown in Fig. 3(c), R_s represents the solution resistance, and Q_r and R_r indicate the capacitance and resistance of the surface corrosion product, respectively. Q_{dl} and R_{ct} represent the capacitance and resistance of the double charge layer, respectively. The EIS fitting parameters of 316 SS are listed in Table 3. In this study, the reciprocal of the charge transfer resistance ($1/R_{ct}$) was adopted to estimate the corrosion rate of 316 SS under different UV radiation intensities, as shown in Fig. 3(d). The $1/R_{ct}$ values of the 316 SS are all lower than those without UV radiation. When UV radiation intensity was increased from 0.25 mW/cm^2 to 2 mW/cm^2 , the UV radiation effectively restrained the corrosion rate. With further increase in the UV radiation intensity from 0.25 mW/cm^2 to 0.5 mW/cm^2 , the inhibitory influence of UV gradually increased. In contrast, the inhibitory influence of UV radiation gradually decreased when the UV radiation intensity was increased from 0.5 to 2 mW/cm^2 . That is, the inhibitory

influence of UV radiation on the corrosion rate was the strongest when the UV radiation intensity was maintained at 0.5 mW/cm^2 .

3.2 Morphologies of the Corrosion Products

Figure 4 displays the SEM morphologies of the surface corrosion products of 316 SS under different UV radiation intensities for an exposure time of 10 days. As evident in Fig. 4(a), some dispersed corrosion products are formed on the surface of 316 SS in the absence of UV radiation. When UV radiation intensity is increased from 0.25 to 0.5 mW/cm^2 , a small amount of corrosion products are formed, as shown in Fig. 4(b) and (c). However, the content of corrosion products gradually increases with increase in UV radiation intensity from 0.5 to 2 mW/cm^2 , as shown in Fig. 4(d) and (e).

LSCM simultaneously provides information on the surface morphology and roughness of corrosion products. Figure 5 shows the 3D surface morphologies and surface roughness (Ra) values of 316 SS under different UV radiation intensities for an exposure time of 10 days. All results were obtained for the same parameters and area sizes. At a UV radiation intensity of 0.5 mW/cm^2 , the Ra value of 316 SS is approximately 0.360 μm (Fig. 5a). When the UV radiation intensity was increased from 0.25 mW/cm^2 to 0.5 mW/cm^2 , the Ra value of 316 SS gradually decreased and reached a minimum value of 0.116 μm , as shown in Fig. 5(b) and (c). Then, the Ra value gradually increases when the UV radiation intensity was increased from 0.5 mW/cm^2 to 2 mW/cm^2 , as shown in Fig. 5(d) and (e).

Table 3 The fitting results of EIS parameters

Parameter		$R_s, \Omega\cdot\text{cm}^2$	Q_r		$R_r, \Omega\cdot\text{cm}^2$	Q_{dl}		$R_{ct}, \Omega\cdot\text{cm}^2$
Conditions			$Y_p, \Omega^{-1}\cdot\text{cm}^{-2}\cdot\text{S}_n$	n_r		$Y_{dl}, \Omega^{-1}\cdot\text{cm}^{-2}\cdot\text{S}_n$	n_{dl}	
Without UV	2 d	9.535	9.251×10^{-6}	0.7498	62.49	1.392×10^{-5}	0.8401	2.259×10^5
	4 d	17.02	1.19×10^{-5}	0.678	140.3	1.603×10^{-5}	0.7718	9.484×10^4
	6 d	5.697	9.19×10^{-6}	0.7964	26.16	2.366×10^{-5}	0.7973	1.498×10^5
	8 d	7.88	6.83×10^{-6}	0.791	35.72	1.659×10^{-5}	0.7919	1.596×10^5
	10 d	6.748	7.09×10^{-6}	0.7921	26.56	1.741×10^{-5}	0.7853	1.53×10^5
UV 0.25	2 d	15.34	1.19×10^{-5}	0.7041	108.4	1.606×10^{-5}	0.8076	7.94×10^4
	4 d	13.89	1.22×10^{-5}	0.709	94.39	1.476×10^{-5}	0.8211	1.935×10^5
	6 d	10.1	1.071×10^{-5}	0.7325	61.08	1.445×10^{-5}	0.8259	2.367×10^5
	8 d	9.48	9.822×10^{-6}	0.7347	53.3	1.532×10^{-5}	0.8056	3.24×10^5
	10 d	8.542	7.858×10^{-6}	0.7608	42.97	1.685×10^{-5}	0.7964	2.964×10^5
UV 0.5	2 d	11.08	7.27×10^{-6}	0.7931	62.53	1.69×10^{-5}	0.8649	1.2×10^5
	4 d	8.943	6.1×10^{-6}	0.8176	46.37	1.57×10^{-5}	0.871	3.08×10^5
	6 d	7.881	6.46×10^{-6}	0.8179	39.96	1.66×10^{-5}	0.8534	3.56×10^5
	8 d	6.468	6.87×10^{-6}	0.8236	27	1.88×10^{-5}	0.8436	4.29×10^5
	10 d	5.706	6.53×10^{-6}	0.8341	22.35	1.9×10^{-5}	0.842	4.33×10^5
UV 1	2 d	21.64	1.6×10^{-5}	0.6761	166.6	2.83×10^{-5}	0.7511	9.14×10^4
	4 d	11.82	8.39×10^{-6}	0.7549	65.21	1.52×10^{-5}	0.8099	2.13×10^5
	6 d	7.05	5.51×10^{-6}	0.8249	32.58	1.53×10^{-5}	0.8399	3.13×10^5
	8 d	10.2	6.11×10^{-6}	0.81	37.39	1.81×10^{-5}	0.8379	3.28×10^5
	10 d	9.029	6.38×10^{-6}	0.8048	39.5	1.58×10^{-5}	0.8307	3.23×10^5
UV 2	2 d	8.371	2.97×10^{-5}	0.6569	83.56	1.87×10^{-5}	0.8139	8.49×10^4
	4 d	7.088	1.29×10^{-5}	0.746	42.78	2.61×10^{-5}	0.789	1.16×10^5
	6 d	6.413	1.09×10^{-5}	0.7669	34.12	2.64×10^{-5}	0.7892	1.62×10^5
	8 d	5.357	9.86×10^{-6}	0.7829	24.9	2.53×10^{-5}	0.7856	1.88×10^5
	10 d	5.638	8.5×10^{-6}	0.7935	25.15	2.25×10^{-5}	0.7923	2.60×10^5

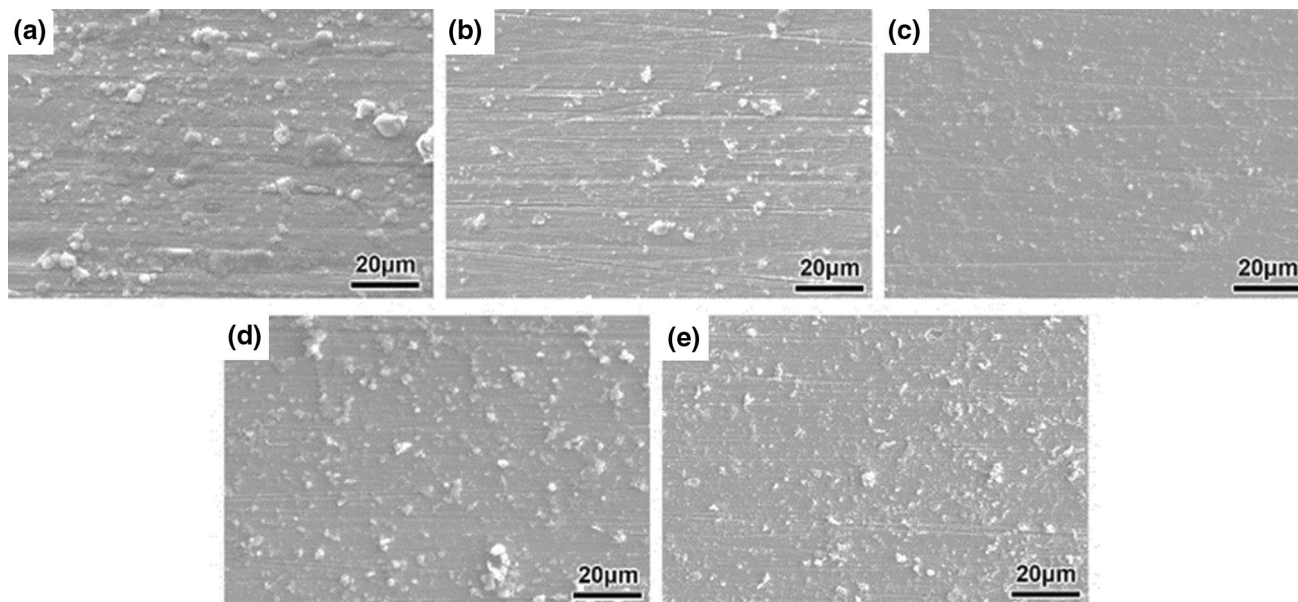


Fig. 4 SEM images of 316 SS after 10 days of corrosion under UV radiation intensity of (a) 0 mw/cm², (b) 0.25 mw/cm², (c) 0.5 mw/cm², (d) 1 mw/cm², and (e) 2 mw/cm²

3.3 XPS of Corrosion Products

Figure 6 shows the XPS spectra of 316 SS under different UV radiation intensities for an exposure time of 10 days. In

particular, the figure shows Fe 2p_{2/3}, Cr 2p_{2/3}, and O 1s core-level peaks. The XPS results confirm that Fe element is mainly presented as Fe_{metal}, Fe_{ox}²⁺, Fe_{ox}³⁺, Fe_{hyd}, and Fe_x (LDH,

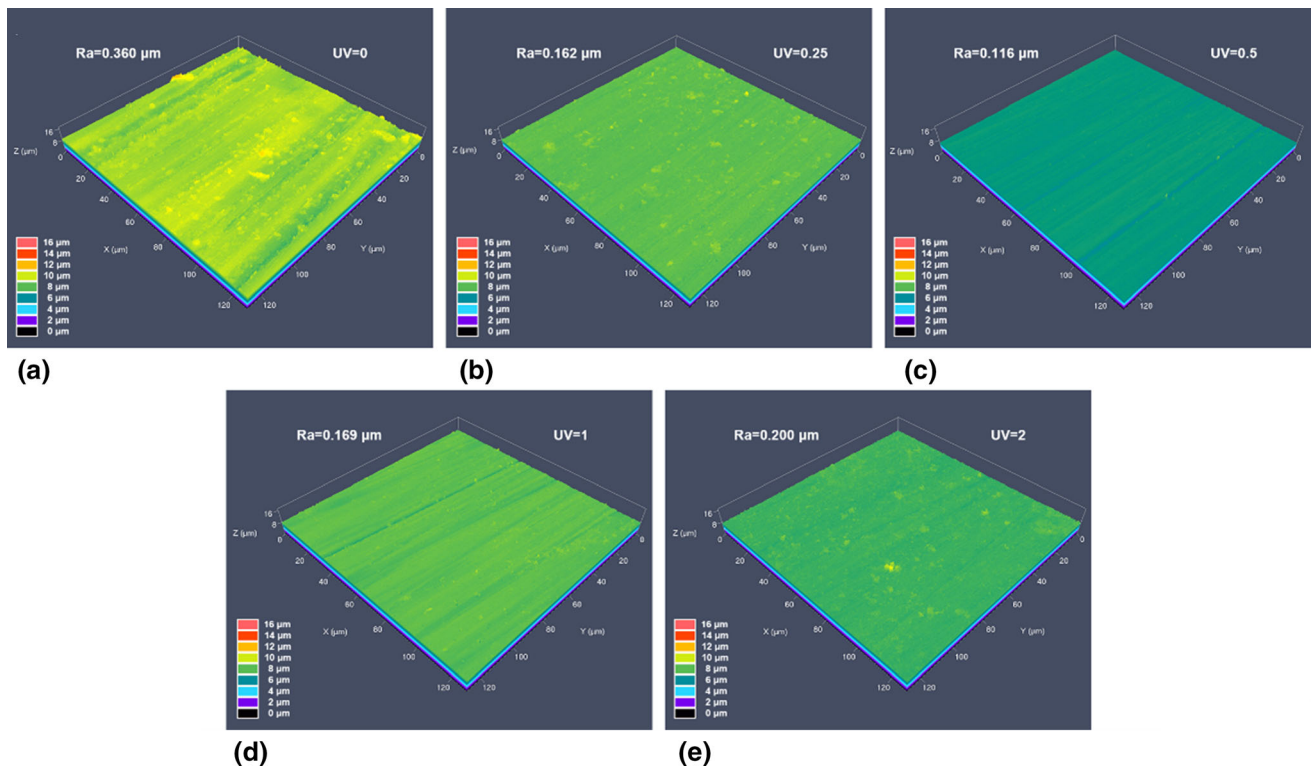


Fig. 5 LSCM images along with 3D surface roughness values of the surface of 316 SS after 10 days of corrosion under UV radiation intensity of (a) 0 mW/cm^2 , (b) 0.25 mW/cm^2 , (c) 0.5 mW/cm^2 , (d) 1 mW/cm^2 , and (e) 2 mW/cm^2

layered double hydroxides) with binding energies of 707.2, 709.4, 710.7, 711.7, and 713.2 eV, respectively (Fig. 6a and b). Similarly, the Cr 2p_{2/3} peaks are mainly distributed at 574.6, 576.4, 577.4, and 578.8 eV, which are assigned to be Cr_{metal}, Cr_{ox}³⁺, Cr_{hyd}, and Cr_{ox}⁶⁺ (Fig. 6c and d). The O 1s peaks are mainly attributed to O²⁻, OH, and H₂O with binding energies of 530.3, 531.2, and 532.5 eV, respectively. (Fig. 6e and f). The fitting parameters for the XPS results are listed in Table 4 (Ref 25-27). The XPS results indicated that UV radiation intensities did not change the type of corrosion products; however, it varied their relative content on the surface of 316 SS.

Figure 7 shows the relative contents of hydroxide and oxide in the main Fe and Cr compounds of the corrosion products under different UV radiation intensities. Notably, the relative amount of [Fe_{ox}] in corrosion products was remarkably higher under UV radiation than that in the absence of UV radiation, while a reverse trend was observed for [Fe_{hyd}]. These results indicate that UV radiation restrained the production of Fe_{hyd} and promoted the production of [Fe_{ox}] to some extent. Similarly, UV radiation also influenced the relative content of Cr compounds in the corrosion products. The relative content of Cr_{ox}³⁺ under different UV radiation intensities was higher than that in the absence of UV radiation. At a UV radiation intensity of 0.5 mW/cm^2 , the relative content of Cr_{ox}³⁺ apparently increased, whereas the relative content of Cr_{hyd} appeared to be less than that without UV irradiation. Previous

studies suggest that Cr₂O₃ thin layers are relatively compact in nature and display excellent protective effect, while the Cr(OH)₃ thin layer is relatively porous and displays poor protective effect (Ref 28). Thus, when the UV radiation intensity is 0.5 mW/cm^2 , the high content of Cr₂O₃ in the corrosion products is beneficial for enhancing the corrosion resistance of 316 SS. Therefore, the strongest inhibitory influence of UV radiation observed on the corrosion rate at the UV radiation intensity of 0.5 mW/cm^2 may be related to the enhanced protective effect of corrosion products. For a UV radiation intensity of 2 mW/cm^2 , the relative content of Cr_{hyd} apparently became higher than that in the absence of UV radiation, while in the case of Cr_{ox}³⁺, the reverse trend was observed. Thus, the inhibitory influence of UV radiation gradually decreased when the UV radiation intensity was increased from 0.5 to 2 mW/cm^2 .

The above results indicate that UV radiation affected the relative content of corrosion products and inhibited the corrosion rate of 316 SS under different UV radiation intensities. Moreover, the inhibitory effect could be closely related to the intensity of UV radiation. The ratio of [Cr]/{[Cr]+[Fe]} in the corrosion products under different UV radiation intensities was further calculated, and the corresponding results are plotted in Fig. 8. The ratio of [Cr]/{[Cr]+[Fe]} under different UV radiation intensities was greater than that in the absence of UV radiation. A higher ratio of [Cr]/{[Cr]+[Fe]}

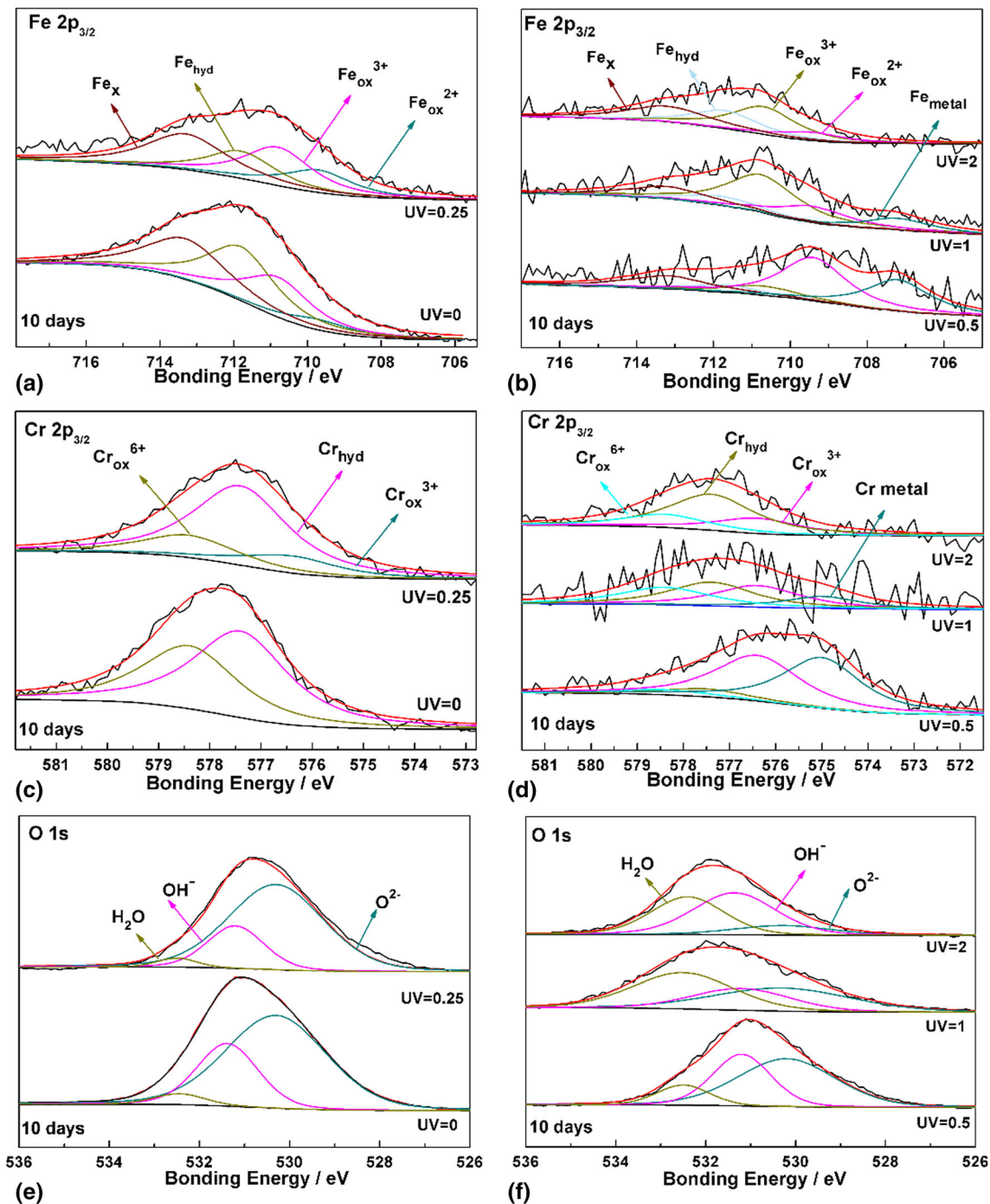


Fig. 6 XPS spectra observed for 316 SS under different UV radiation intensities after 10 days of corrosion in Fe 2p_{3/2}, Cr 2p_{3/2} and O 1s

in the passive film can enhance the corrosion resistance of stainless steel (Ref 29, 30). Fujimoto et al. found that Cr was selectively enriched in the passive film under UV radiation, thus inhibiting pitting corrosion on stainless steel surfaces (Ref 31). In this study, further enrichment of Cr content in the corrosion products by UV radiation is supposed to be the main factor affecting the corrosion rate of 316 stainless steel under

UV radiation. The ratio of $[\text{Cr}]/\{[\text{Cr}]/[\text{Fe}]\}$ initially increased and then decreased with a change in UV radiation intensity range of 0.25-2 mW/cm². Thus, when the UV radiation intensity is 0.5 mW/cm², the high ratio of $[\text{Cr}]/\{[\text{Cr}]/[\text{Fe}]\}$ in the corrosion products is beneficial for enhancing the corrosion performance of 316 SS.

3.4 Analysis of Pits Morphology and Depth

Figures 9 and 10 shows the pit morphologies and pit sizes (depth and density) of 316 SS under different UV radiation intensities for an exposure time of 10 days. The maximum pit depth formed on the surface of stainless steel is closely related to the safety of stainless steel in service. Therefore, the maximum pit depth was analyzed using a statistical analysis method. Figure 10(a) presents the largest pit depth formed on 316 SS under different UV radiation intensities for an exposure time of 10 days. The maximum pit depth initially decreased gradually and then increased as UV radiation intensity changed in the range 0.25-2 mW/cm². The maximum pit depth, formed on 316 SS under UV radiation intensities, was smaller than that without UV irradiation. The maximum pit depth was the smallest when the UV radiation intensity is 0.5 mW/cm². In addition, Fig. 10(b) shows the pit density formed on 316 SS under different UV radiation intensities. The change in pit density followed a similar trend as that of the pit depth.

Table 4 Parameters of XPS spectra

Elements	Chemical state	Binding Energy, eV	FWHA*, eV
Fe	Fe(metal)	707.2	2
	Fe _{ox} ²⁺	709.4	2.2
	Fe _{ox} ³⁺	710.7	2.2
	Fe _{hyd}	711.7	2.2
	LDH	713.2	2.6
Cr	Cr(metal)	574.6	2
	Cr _{ox} ³⁺	576.4	2.2
	Cr _{hyd}	577.4	2.2
	Cr _{ox} ⁶⁺	578.8	2.2
O	O ²⁻	530.3	2.6
	OH ⁻	531.2	1.5
	H ₂ O	532.5	1.4

4. Conclusions

In this study, the influence of different UV radiation intensities on the corrosion performance of 316 SS was studied in a simulated salt-lake environment. The main conclusions of this work are as follows:

1. The EIS results revealed that the corrosion rate of 316 SS was apparently inhibited by UV radiation, and the influence of this UV inhibition phenomenon initially increased and then decreased with increasing the UV radiation intensity from 0.25 to 2 mW/cm². The inhibition effect of UV on the corrosion rate of 316 SS was the strongest when the UV radiation intensity was 0.5 mW/cm².
2. UV radiation intensities did not change the type of surface corrosion products of 316 SS during the corrosion

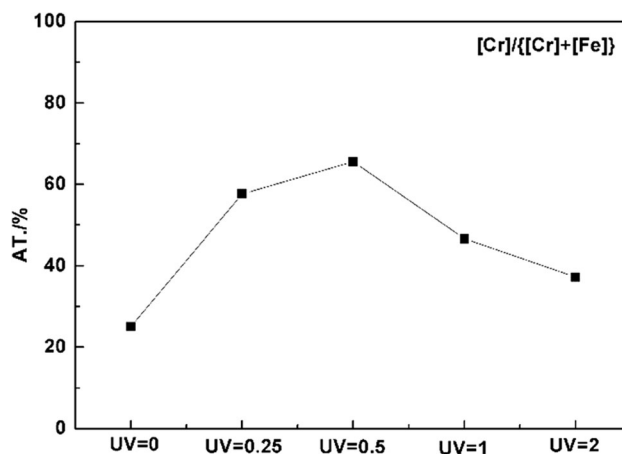


Fig. 8 The ratio of [Cr]/{[Cr]+[Fe]} in corrosion products of 316 SS under different UV radiation intensities after 10 days of corrosion

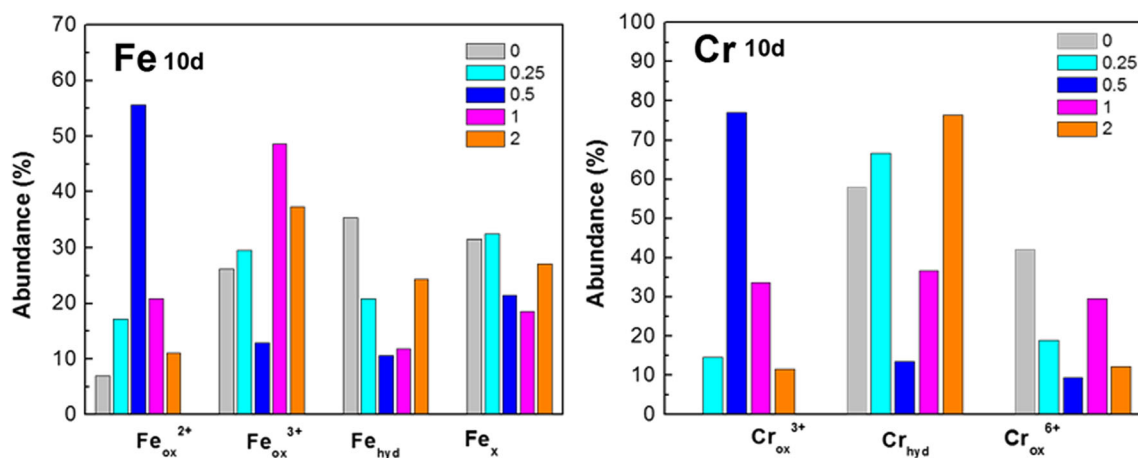


Fig. 7 The relative contents of “hydroxide” and “oxide” in primary Fe and Cr compounds of surface corrosion products of 316 SS under different UV radiation intensities after 10 days of corrosion

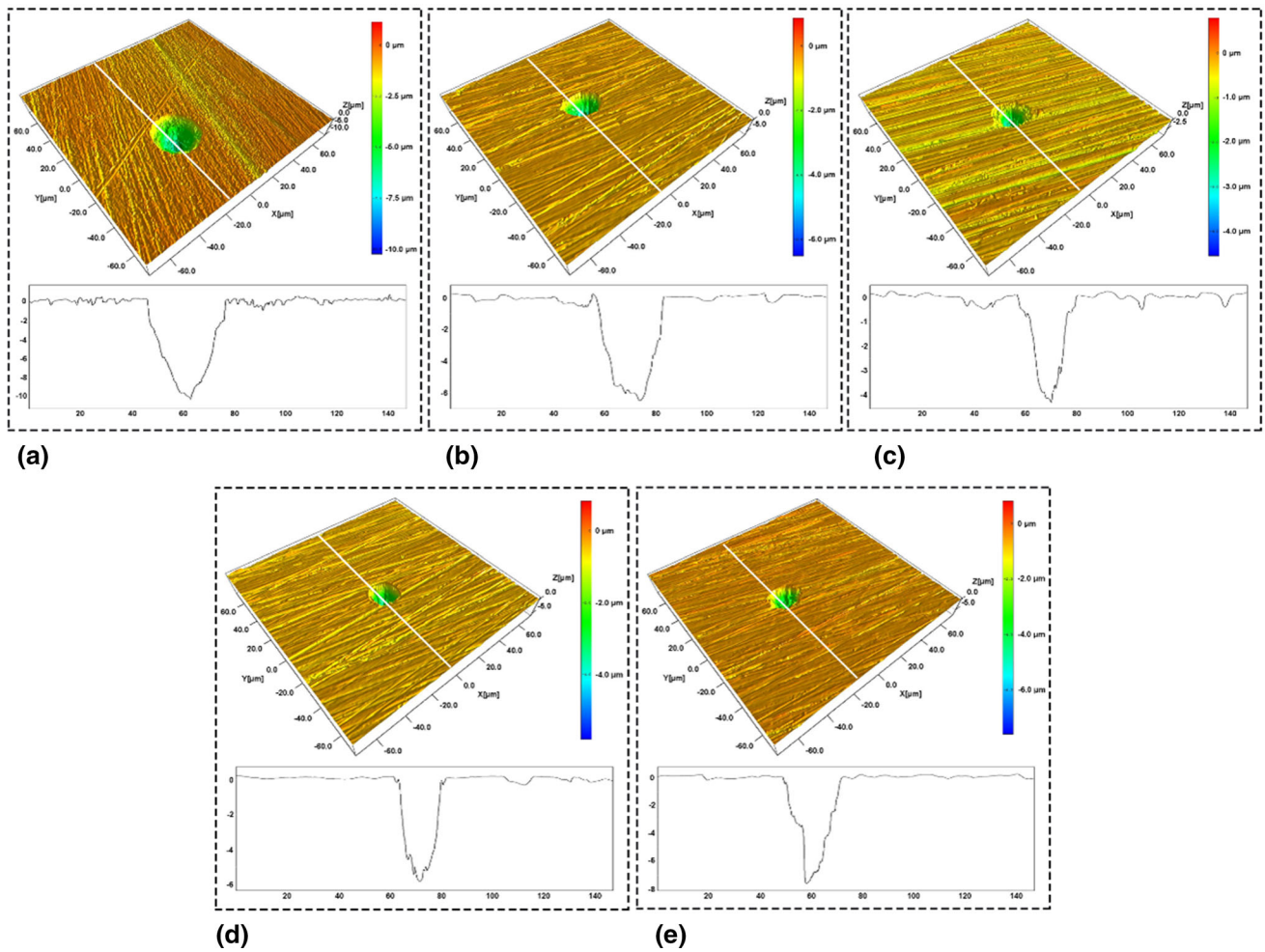


Fig. 9 Representative morphologies of pits formed on 316 SS after 10 days of corrosion under UV radiation intensity of (a) 0 mw/cm^2 , (b) 0.25 mw/cm^2 , (c) 0.5 mw/cm^2 , (d) 1 mw/cm^2 , and (e) 2 mw/cm^2

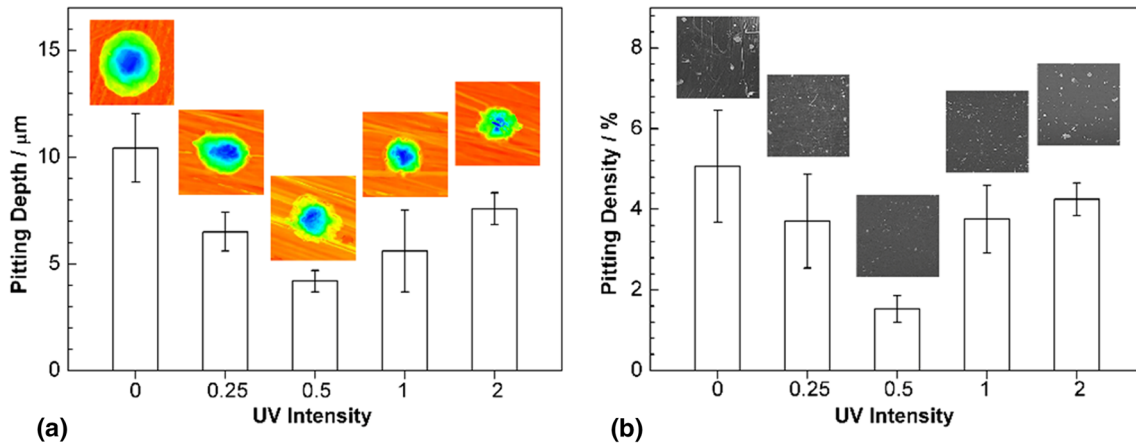


Fig. 10 Maximum pit depth (a) and pit density (b) of 316 SS under different UV radiation intensities after 10 days of corrosion

process; however, it altered the relative composition of the corrosion products. The increasing ratio of $[\text{Cr}]/\{[\text{Cr}] + [\text{Fe}]\}$ in the corrosion products could improve the protection ability of the corrosion products formed on 316 SS.

3. The maximum pit depth and pit density formed on the surface of 316 SS initially decreased gradually and then increased with a change in UV radiation intensity range of $0.25\text{-}2 \text{ mW/cm}^2$.

Acknowledgments

Thanks to Prof. Zhuoyuan Chen of Foshan University for his scientific comments on this paper. The investigation is supported by National Natural Science Foundation of China (No. 51671197) and Liaoning Shenyang Soil and Atmosphere Corrosion of Material National Observation and Research Station.

References

1. D.B. Blucher, J.E. Svensson, L.G. Johansson et al., The NaCl-Induced Atmospheric Corrosion of Aluminum - The Influence of Carbon Dioxide and Temperature, *J. Electrochem. Soc.*, 2003, **150**(3), p B93–B98
2. C.G. Soares, Y. Garbatov, A. Zayed et al., Influence of Environmental Factors on Corrosion of Ship Structures in Marine Atmosphere, *Corros. Sci.*, 2009, **51**(9), p 2014–2026
3. C. Qiao, M.N. Wang, L. Hao et al., Temperature and NaCl Deposition Dependent Corrosion of SAC305 Solder Alloy in Simulated Marine Atmosphere, *J. Mater. Sci. Technol.*, 2021, **75**, p 252–264
4. F. Mansfeld and J.V. Kenkel, Electrochemical Measurements of Time-of-Wetness and Atmospheric Corrosion Rates, *Corrosion*, 2013, **33**(1), p 13–16
5. C.L. Li, Y.T. Ma, Y. Li et al., EIS Monitoring Study of Atmospheric Corrosion Under Variable Relative Humidity, *Corros. Sci.*, 2010, **52**(1), p 3677–3686
6. A.P. Yadav, A. Nishikata and T. Tsuru, Electrochemical Impedance Study on Galvanized Steel Corrosion Under Cyclic Wet-Dry Conditions-Influence of Time of Wetness, *Corros. Sci.*, 2004, **46**(1), p 169–181
7. E. Schindelholz, R.G. Kelly, I.S. Cole et al., Comparability and Accuracy of Time of Wetness Sensing Methods Relevant for Atmospheric Corrosion, *Corros. Sci.*, 2013, **67**, p 233–241
8. M. Mouanga and P. Bercot, Comparison of Corrosion Behaviour of Zinc in NaCl and in NaOH Solutions; Part II: Electrochemical Analyses, *Corros. Sci.*, 2010, **52**(12), p 3993–4000
9. M. Mouanga, P. Bercot and J.Y. Rauch, Comparison of Corrosion Behaviour of Zinc in NaCl and in NaOH Solutions. Part I: Corrosion Layer Characterization, *Corros. Sci.*, 2010, **52**(12), p 3984–3992
10. J.B. Zhang, J. Wang and Y.H. Wang, The Deliquescence and Spreading of Sea Salt Particles on Carbon Steel and Atmospheric Corrosion, *Mar. Sci.*, 2005, **29**(7), p 17–19
11. L.Y. Song and Z.Y. Chen, The Role of UV Illumination on the NaCl-Induced Atmospheric Corrosion of Q235 Carbon Steel, *Corros. Sci.*, 2014, **86**, p 318–325
12. E.A. Thompson and T.D. Burleigh, Accelerated Corrosion of Zinc Alloys Exposed to Ultraviolet Light, *Corros. Eng. Sci. Techn.*, 2007, **42**(3), p 237–241
13. Y.W. Liu, J. Zhang, Y.H. Wei et al., Effect of Different UV Intensity on Corrosion Behavior of Carbon Steel Exposed to Simulated Nansha Atmospheric Environment, *Mater. Chem. Phys.*, 2009, **237**, p 121855
14. C.B. Breslin, D.D. Macdonald, J. Sikora et al., Influence of UV Light on the Passive Behaviour of SS316 - Effect of Prior Illumination, *Electrochim. Acta*, 1997, **42**(1), p 127–136
15. S.O. Moussa and M.G. Hocking, The Photo-Inhibition of Localized Corrosion of 304 Stainless Steel in Sodium Chloride Environment, *Corros. Sci.*, 2001, **43**(11), p 2037–2047
16. M.X. Guo, Q. Yin, M.R. Liu et al., Corrosion Behavior of 304 Stainless Steel Exposed to a Simulated Salt Lake Atmosphere, *Acta. Metall. (Sin.-Engl.)*, 2020, **33**(6), p 857–870
17. T. Shinohara, S. Motoda and W. Oshikawa, Evaluation of Corrosivity in Atmospheric Environment by ACM (Atmospheric Corrosion Monitor) Type Corrosion Sensor, *Mater. Sci. Forum*, 2005, **475**, p 61–64
18. D. To, T. Shinohara, O. Umezawa et al., Experimental Investigation on the Corrosivity of Atmosphere through the Atmospheric Corrosion Monitoring (ACM) Sensors, *Electrochem. Soc.*, 2017, **75**(29), p 1–10
19. D. Mizuno, S. Suzuki, S. Fujita et al., Corrosion Monitoring and Materials Selection for Automotive Environments by Using Atmospheric Corrosion Monitor (ACM) Sensor, *Corros. Sci.*, 2014, **83**, p 217–225
20. A.K. Neufeld, I.S. Cole, A.M. Bond et al., The Initiation Mechanism of Corrosion of Zinc by Sodium Chloride Particle Deposition, *Corros. Sci.*, 2002, **44**(3), p 555–572
21. C. Pan, W.Y. Ly, Z.Y. Wang et al., Atmospheric Corrosion of Copper Exposed in a Simulated Coastal-Industrial Atmosphere, *J. Mater. Sci. Technol.*, 2017, **33**(6), p 587–595
22. A. Nishikata, Y. Ichihara and T. Tsuru, An Application of Electrochemical Impedance Spectroscopy to Atmospheric Corrosion Study, *Corros. Sci.*, 1995, **37**(6), p 897–911
23. X.N. Liao, F.H. Cao, A.N. Chen et al., In-Situ Investigation of Atmospheric Corrosion Behavior of Bronze Under Thin Electrolyte Layers Using Electrochemical Technique, *T. Nonferr. Metal. Soc.*, 2012, **22**(5), p 1239–1249
24. C. Qiao, X. Sun, Y.Z. Wang et al., A Perspective on Effect by Ag Addition to Corrosion Evolution of Pb-Free Sn Solder, *Mater. Lett.*, 2021, **297**, p 129935
25. W. Lv, C. Pan, W. Su, Z. Wang et al., Atmospheric Corrosion Mechanism of 316 Stainless Steel in Simulated Marine Atmosphere, *Corros. Eng. Sci. Technol.*, 2016, **51**(3), p 155–162
26. D. Kong, X. Ni, C. Dong et al., Bio-Functional and Anti-Corrosive 3D Printing 316L Stainless Steel Fabricated by Selective Laser Melting, *Mater. Des.*, 2018, **152**, p 88–101
27. R.-H. Jung, H. Tsuchiya and S. Fujimoto, Growth Process of Passive Films on Austenitic Stainless Steels under Wet-dry Cyclic Condition, *ISIJ Int.*, 2012, **52**(7), p 1356–1361
28. T. Ishitsuka and K. Nose, Stability of Protective Oxide Films in Waste Incineration Environment - Solubility Measurement of Oxides in Molten Chlorides, *Corros. Sci.*, 2002, **44**(2), p 247–263
29. K. Asami and K. Hashimoto, Importance of Initial Surface Film in the Degradation of Stainless Steels by Atmospheric Exposure, *Corros. Sci.*, 2003, **45**(10), p 2263–2283
30. Z.X. Li, L.M. Zhang, A.L. Ma et al., Comparative Study on the Cavitation Erosion Behavior of Two Different Rolling Surfaces on 304 Stainless Steel, *Tribol. Int.*, 2021, **159**, p 106994
31. S. Fujimoto, T. Yamada and T. Shibata, Improvement of Pitting Corrosion Resistance of Type 304 Stainless Steel by Modification of Passive Film with Ultraviolet Light Irradiation, *J. Electrochem. Soc.*, 1998, **145**(5), p L79–L81

Publisher's Note Springer Nature remains neutral with regard to jurisdictional claims in published maps and institutional affiliations.